

# Deflection Analysis of the Space Shuttle External Tank Door Drive Mechanism

Michael A. Tosto<sup>\*</sup>, Bo C. Trieu<sup>\*\*</sup>, Brent A. Evernden<sup>+</sup>,  
Drew J. Hope<sup>\*\*</sup>, Kenneth A. Wong<sup>+</sup>, Robert E. Lindberg<sup>\*</sup>

## Abstract

Upon observing an abnormal closure of the Space Shuttle's External Tank Doors (ETD), a dynamic model was created in MSC/ADAMS to conduct deflection analyses for assessing whether the Door Drive Mechanism (DDM) was subjected to excessive additional stress, and more importantly, to evaluate the magnitude of the induced step or gap with respect to shuttle's body tiles. To model the flexibility of the DDM, a lumped parameter approximation was used to capture the compliance of individual parts within the drive linkage. These stiffness approximations were then validated using FEA and iteratively updated in the model to converge on the actual distributed parameter equivalent stiffnesses. The goal of the analyses is to determine the deflections in the mechanism and whether or not the deflections are in the region of elastic or plastic deformation. Plastic deformation may affect proper closure of the ETD and would impact aero-heating during re-entry.

## Introduction

During the Space Shuttle mission STS-118 of August 2007, ground telemetry data indicated that the External Tank Doors (ETD) did not fully complete their travel before final closing uplatches were commanded to engage. Because the DDM actuator has a fail-safe brake which engages when no power is applied, the mechanism is constrained at its input link as the door is forced to close. The constraint at the input link would effectively create deflection in the DDM linkages and induce associated stress. This action was modeled using the multi-body dynamics software MSC/ADAMS. To represent each flexible part, single degree of freedom linear springs were introduced for links in tension and compression, while torsional springs at the base of rigid cranks were used for links in bending. With the door drive input crank fixed, the door was then forced to close, thereby simulating the conditions seen by the actual mechanism. Using the ratio of FEA stresses calculated based on spring deflection and spring force, the stiffness of each link was updated until convergence on the actual equivalent stiffness. In addition to this deflection analysis, a tolerance analysis was performed on the DDM to determine the observable effect of joint tolerance stackup at the door's outboard edge.

## Background

The ETD cover openings in the orbiter's underside are access regions for the umbilical and structural connections between the External Tank (ET) and orbiter. The ETD sits at the aft underside of the orbiter, and is prominently visible in its open configuration in Figure 1.

---

<sup>\*</sup> National Institute of Aerospace/University of Virginia, Hampton, VA

<sup>\*\*</sup> NASA Langley Research Center, Hampton, VA

<sup>+</sup> NASA Johnson Space Center, Houston, TX



**Figure 1. OV-103, *Discovery*, Before STS-114**

After jettisoning the ET during ascent, these doors are closed while on orbit and remain closed throughout the duration of flight and descent, until they are opened after landing for inspection. Proper door closure is critical to avoid excessive aero-heating during descent through the Earth's atmosphere. Thermal analysis has shown that if the doors are not fully closed and aligned with surrounding TPS tiles within 3.8 mm (0.15 in), a safe descent would be questioned [1].

The three main ETD subsystems are the Centerline Latches (CL), Door Drive Mechanism (DDM), and Uplatch Mechanism (UM). The CL locks the doors in their open configuration while the ET is connected to the orbiter and through out the ascent stage. With the ET jettisoned, and while in orbit, the DDM is commanded to move both doors from their open to closed configuration. Finally the UM, which has three hooks, is activated to latch the doors in their closed configuration and compresses the thermal and pressure seals for proper closure. Figure 2 shows a close-up of the starboard-side door with the DDM and the three hooks of the UM highlighted.

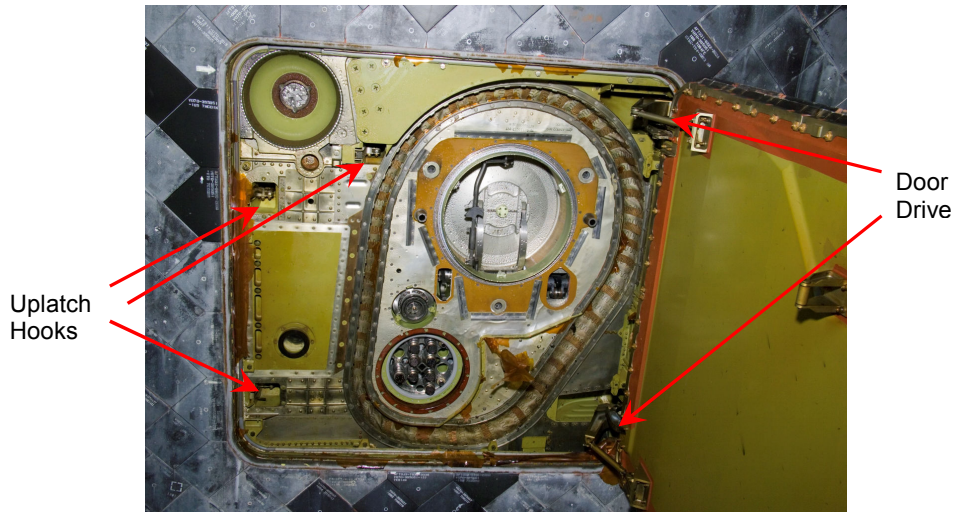


**Figure 2. Close-Up of ETD Showing Uplatch Hooks and Door Drive**

A Pro/E CAD model of the port-side ETD including the DDM and UM in its closed and latched configuration is shown in Figure 3. Actuators are not shown.

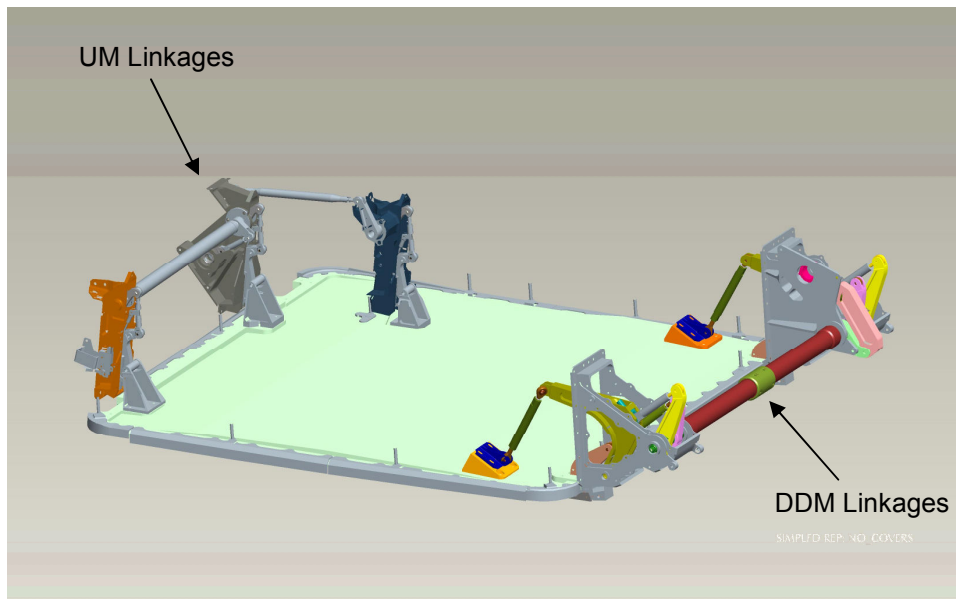


**Figure 3. Port Side ET Door Configuration including DDM & UM**

### Analytical Approach

#### Simulation to Obtain Deflections

Because the first set of ready-to-latch indications were obtained, the door was within the capture envelope of the UM and therefore within 51 mm (2 in) of closure. Latching the doors with the DDM's actuator brake is on will induce deflection in the mechanism. The primary goal is to determine deflections in the DDM linkages. From these deflections, linkage stresses can be computed to determine if deformations are within the elastic or plastic regions. For elastic deformations, cycling the ETD's DDM and UM mechanism will return the door to its final closed configuration with respect to the Shuttle as

expected. If plastic deformations have occurred then the door may form gaps or a step with respect to the Shuttle.

The Pro/E model of the DDM in Figure 3 was initially provided, and used as a starting point for subsequent analysis. This model was then imported to the multi-body dynamics simulation software MSC/ADAMS. As shown in Figure 4, the door rods within ADAMS are a simplified geometric representation of the actual linkage. For the purpose of the mechanism analyses, it is sufficient to represent these links as rod elements with revolute joints at each end.

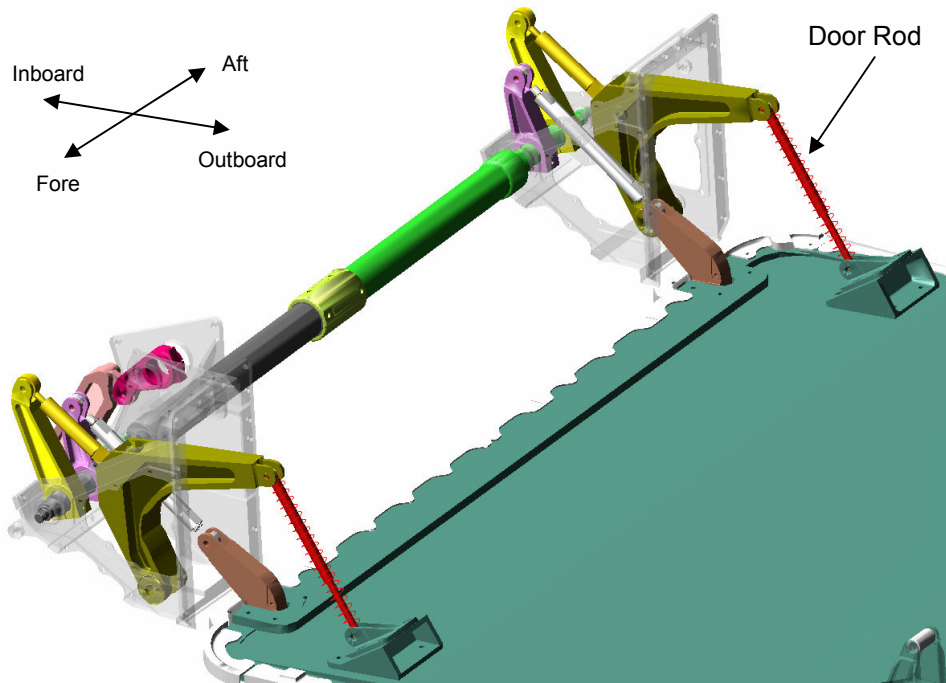


**Figure 4. ETD Door Drive Mechanism**

For deflection analyses, the linkages of the DDM can be represented in ADAMS as spring or compliant members, while the door and shuttle frame are considered rigid. Figure 5 shows each part of the linkage and its spring equivalence depending on loading: linear springs are used for tension or compression and torsional springs (at the base of a rigid crank) for bending. For the “follower 1” part, both compression and bending loads exist, thus linear and torsional springs are used respectively.

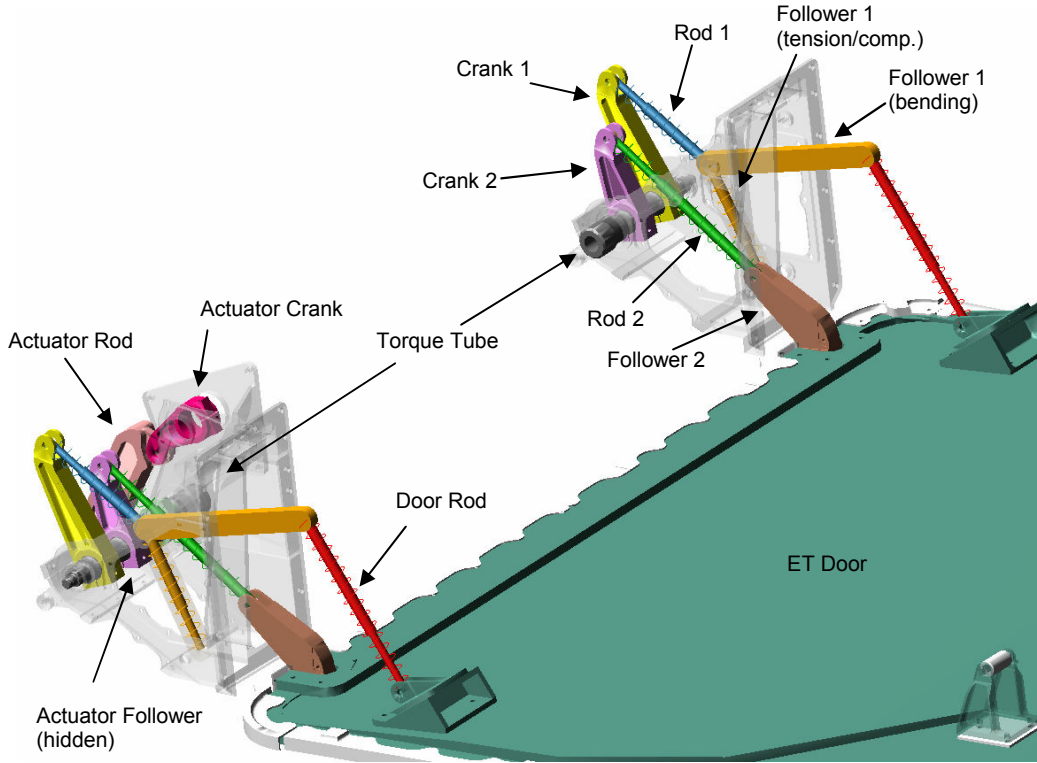


**Figure 5. Spring/Compliant Representation of the DDM**

To find equivalent stiffnesses for use in this lumped parameter model, a representative cross section of each part was taken near its midpoint and used to find values of  $A$  for linear springs and  $I$  for torsional springs. Linear stiffness was found using equation (1) for a rod under axial load [2], and torsional stiffness was found using equation (2) for a cantilever beam with end load, assuming small deflections.

$$k_{eq} = \frac{EA}{l} \left[ \frac{\text{N}}{\text{mm}} \right] \quad (1)$$

$$k_{eq} = l^2 \left( \frac{3EI}{l^3} \right) \left( \frac{\pi}{180} \right) \left[ \frac{\text{N} \cdot \text{mm}}{\text{deg}} \right] \quad (2)$$

To run the dynamic simulation, the actuator crank is fixed (motor brake is on) while the opposing edge of the door is forced to move in the closing direction 25 mm (1 in). According to the door's rigging specifications, actuation the DDM must leave the door between 25.4 mm (1 in) and 44.45 mm (1.75 in) of the fully closed and latched configuration [3]. Therefore, if the door were to stop short at 50.8 mm (2 in), then the maximum amount of additional displacement would be 25.4 mm, if the door were rigged to its minimum sag of 25.4 mm. Figure 6 shows this requirement, as presented in the ETD installation and rigging procedure [3].

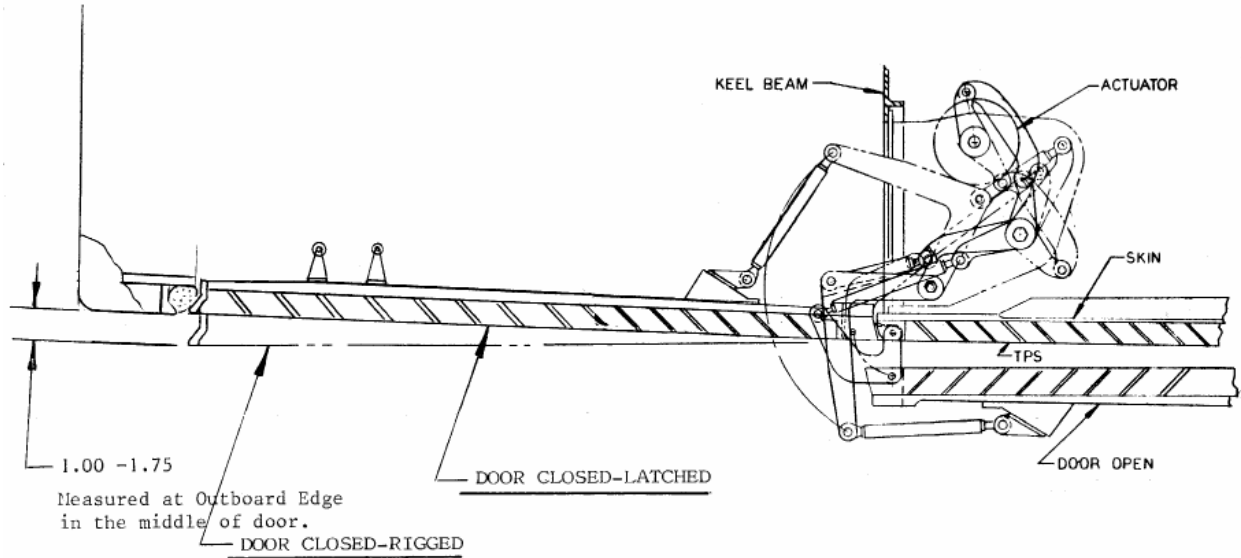


**Figure 6. Port-side Door Looking FWD, Door Sag Specification**

#### Iteration of Stiffness Approximations

If FEA is used to find stress in each component based on the results of dynamic simulation, this corresponds to a switch from a lumped parameter model in MSC/ADAMS to a distributed model in MSC/NASTRAN. While the resulting deflections and forces are analytic within ADAMS, where force and displacement for each linkage obey Hook's law for a given equivalent stiffness, stresses computed in FEA using boundary conditions (BC's) based on these displacements and forces will be different unless the equivalent stiffness is the same in both models. In a linear static analysis, stress is proportional to force, therefore the ratio of stresses in these two load cases is equal to the ratio of applied force respectively. Equation (3) shows this relationship, where the subscript "disp" signifies an FEA model with displacement BC's, and "force" signifies an FEA model with force BC's. Similarly, subscripts "f" and "ds" indicate FEA and dynamic simulation respectively. After the initial dynamic simulation and its associated stress reports,  $k_f$  is the only unknown in equation (3).

$$\frac{\sigma_{disp}}{\sigma_{force}} = \frac{F_{disp}}{F_{force}} = \frac{F_f}{F_{ds}} = \frac{k_f x_{ds}}{k_{ds} x_{ds}} \quad (3)$$

An iterative process is employed to ensure that the equivalent stiffnesses  $k_f$  and  $k_{ds}$  are in fact the same (driving equation (3) to equal 1). After an initial set of deflections and forces is obtained from the ADAMS model, these results are used as the input to a NASTRAN model of each flexible component. Using the stress ratio (SR) described above, a new equivalent stiffness for each link is computed according to equation (4). This result is then used to update the ADAMS model, thereby completing the loop of a process which can be repeated until convergence.

$$k_f = \left( \frac{\sigma_{disp}}{\sigma_{force}} \right) k_{ds} \Rightarrow k_{i+1} = \left( \frac{\sigma_{disp,i}}{\sigma_{force,i}} \right) k_i \quad (4)$$

#### Tolerance Analysis

An important point to note is that the previously described dynamic simulation does not take into account any joint tolerances or mechanical backlash that could allow for movement of the ETD without stressing the DDM linkages. To find the maximum possible amount of movement at the door's outer edge due to

joint tolerance stack-up, the problem was formulated using a vector loop approach [4]. Figure 7 shows the actual mechanism with its two dimensional vector representation overlaid in blue.

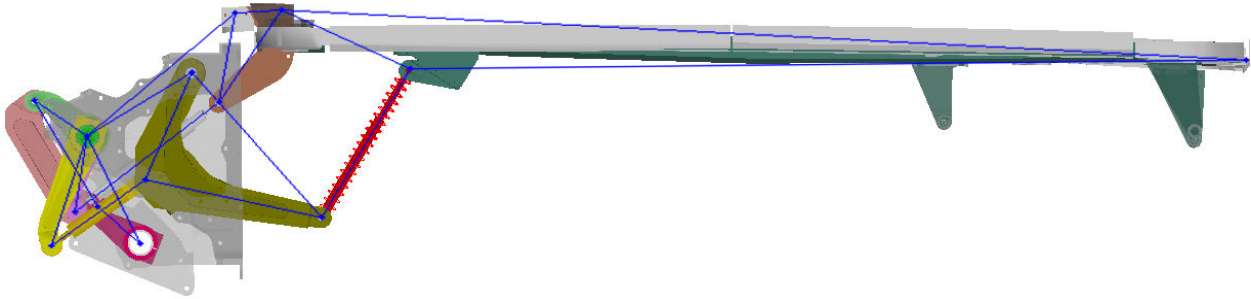


**Figure 7. 2-D Representative Geometry of the DDM**

However, rather than analytically calculating the mechanism's sensitivity to each geometric variation [4], a numerical approach was employed using MATLAB's optimization toolbox. Each vector shown in Figure 7 was given two degrees of freedom, with a constraint placed on its Cartesian length (vector norm). An additional tolerance vector was also inserted between each of the visible link vectors, representing a misalignment of centers at each joint. Because the magnitude of this misalignment may range from zero up to a maximum which is derived from tolerances, constraints on the length of these vectors are implemented as inequalities rather than equalities.

Summation of vector loops is the final critical set of constraints which ensure proper assembly of the mechanism. A sample loop is shown in Figure 8, where a summation of the vectors numbered 1 through 7 (including tolerance vectors at each joint) is required to equal zero. Imposing this constraint on each distinct loop will specify the mechanism topology, and additional slope constraints may be used to remove any ambiguity of inverse kinematics.

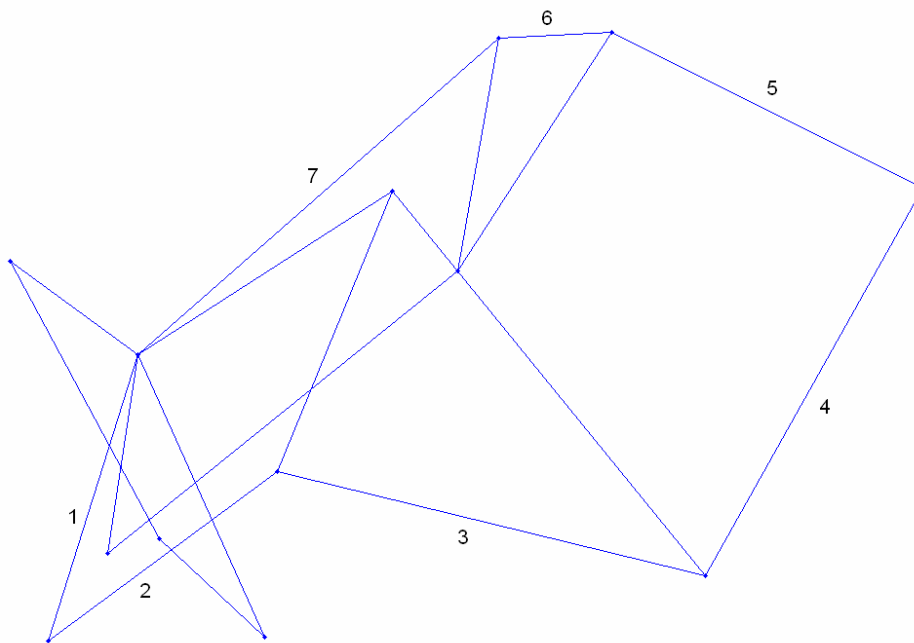


**Figure 8. Vector Loop Summation (Door Removed for Clarity)**

With each vector defined and constrained, the objective function for MATLAB's constrained nonlinear optimization is taken to be the distance of the door's edge from its nominal location.

## Results

### Deflections

Table 1 shows the deflection of each part in the linkage from the initial iteration of ADAMS simulation. These deflections may be used to compute the stress in each linkage member to classify it as either elastic or plastic deformation.

**Table 1. Deflections in the DDM for 25 mm (1 in) at Door Edge**

| Linear Deflections |              |                   | Angular Deflections |                |           |
|--------------------|--------------|-------------------|---------------------|----------------|-----------|
| Location           | Part         | (mm)              | Location            | Part           | (deg)     |
| Aft Hinge          | Follower 1   | 5.67E-02          | Aft Hinge           | Follower 1     | 1.63E+00  |
|                    | Rod 1        | -3.05E-02         |                     | Crank 1        | 3.09E-01  |
|                    | Rod 2        | 5.74E-02          |                     | Crank 2        | -2.54E-01 |
|                    | Door Rod     | -1.74E-01         | Fore Hinge          | Follower 1     | 1.38E+00  |
| Fore Hinge         | Follower 1   | 4.80E-02          |                     | Crank 1        | 2.59E-01  |
|                    | Rod 1        | -2.57E-02         |                     | Crank 2        | -4.76E-01 |
|                    | Rod 2        | 1.08E-01          | Actuator            | Actuator Crank | -2.00E-01 |
| Door Rod           | -1.48E-01    | Actuator Follower |                     | 3.15E-01       |           |
| Actuator           | Actuator Rod | -2.23E-01         | Torque Tube         | Tube           | -2.64E-01 |

(positive = tension, negative = compression)

(positive = fore [right hand rule])

### Convergence of Equivalent Stiffness

Using the previously outlined process, stress ratios were calculated at iteration 0 and compared to the predicted stress ratio, calculated as a stiffness ratio. To find this stiffness ratio, the manually calculated approximate stiffness was used in place of  $k_{ds}$ , and a stiffness found directly from a finite element model (by applying a representative load of 4448 N (1000 lbf) and extracting the displacement) was used in place of  $k_f$ . These values are shown in the columns marked "K ratio [0]" in Table 2 and Table 3. Stress ratio values after one iteration, which should approach 1, are shown in the columns marked " $\sigma$  ratio [1]".

**Table 2. Convergence of Stress Ratios, Links Axially Loaded**

| Location   | Part       | K ratio[0] | $\sigma$ ratio[0] | $\sigma$ ratio[1] |
|------------|------------|------------|-------------------|-------------------|
| Aft Hinge  | Follower 1 |            | 1.016             | 1.011             |
|            | Rod 1      | 0.619      | 0.636             | 1.004             |
|            | Rod 2      | 0.829      | 0.835             | 0.997             |
|            | Door Rod   | 0.829      | 0.832             | 1.009             |
| Fore Hinge | Follower 1 |            | 1.065             | 1.013             |
|            | Rod 1      | 0.619      | 0.632             | 1.002             |
|            | Rod 2      | 0.829      | 0.833             | 0.994             |
|            | Door Rod   | 0.829      | 0.831             | 1.001             |
| Actuator   | Rod        |            | 1.271             | 0.996             |

**Table 3. Convergence of Stress Ratios, Links Loaded in Bending**

| Location   | Part       | K ratio[0] | $\sigma$ ratio[0] | $\sigma$ ratio[1] |
|------------|------------|------------|-------------------|-------------------|
| Aft Hinge  | Follower 1 | 1.701      | 1.806             | 1.061             |
|            | Crank 1    | 1.418      | 1.650             | 0.999             |
|            | Crank 2    | 1.491      | 1.624             | 1.005             |
| Fore Hinge | Follower 1 | 1.701      | 1.793             | 1.062             |
|            | Crank 1    | 1.418      | 1.660             | 1.000             |
|            | Crank 2    | 1.491      | 1.630             | 1.007             |
| Actuator   | Crank      | 1.577      | 1.585             | 1.010             |
|            | Follower   | 1.549      | 1.415             | 1.062             |

Using these results, equivalent stiffnesses can be evaluated for convergence based on stress ratios. If the stress ratio is equal to 1 then the stiffness values used in ADAMS are equal to the equivalent stiffness of the part's finite element model. Therefore, a stress ratio error can be computed by subtracting 1 from all SR values. As this stress ratio error approaches zero, the actual ratio will approach 1. Figure 9 and Figure 10 show the initial SR error values at iteration 0, and the updated SR error values after one iteration. Note that error values greater than 0 signify a part whose stiffness will be increased in the next iteration, while error values less than zero signify a part whose stiffness will be decreased in the next iteration.

**Linear Springs, Stress Ratio Error**

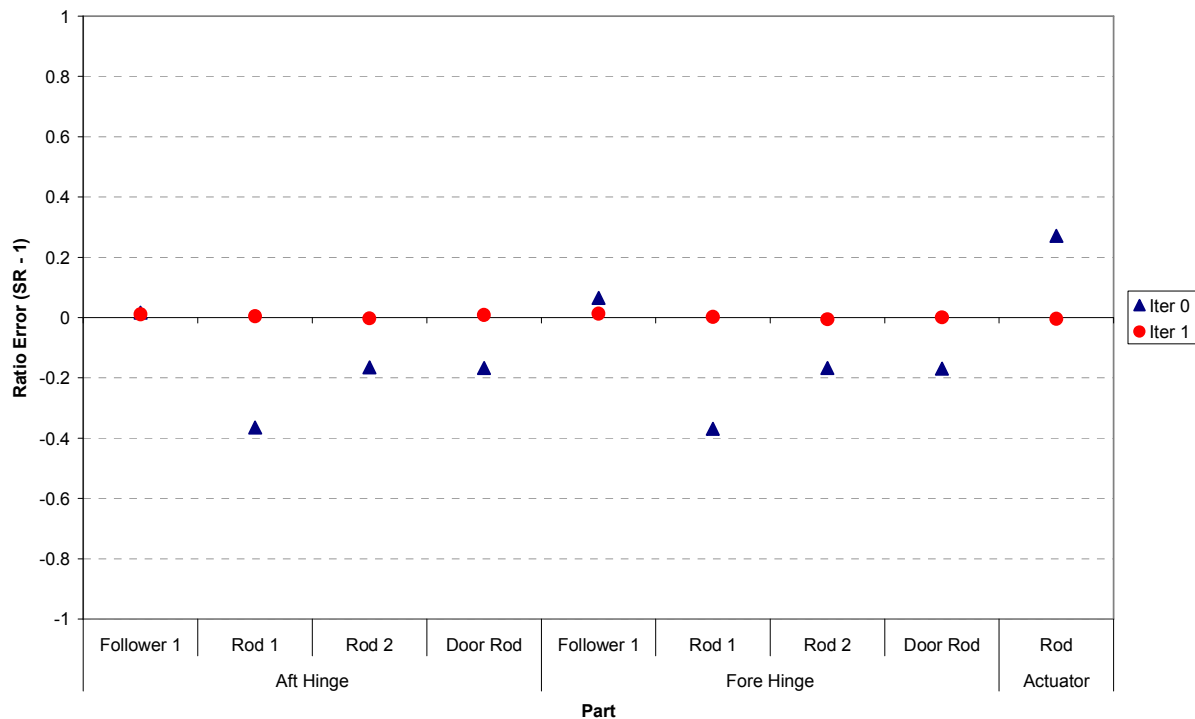


**Figure 9. Stress Ratio in Parts Represented by Linear Springs**

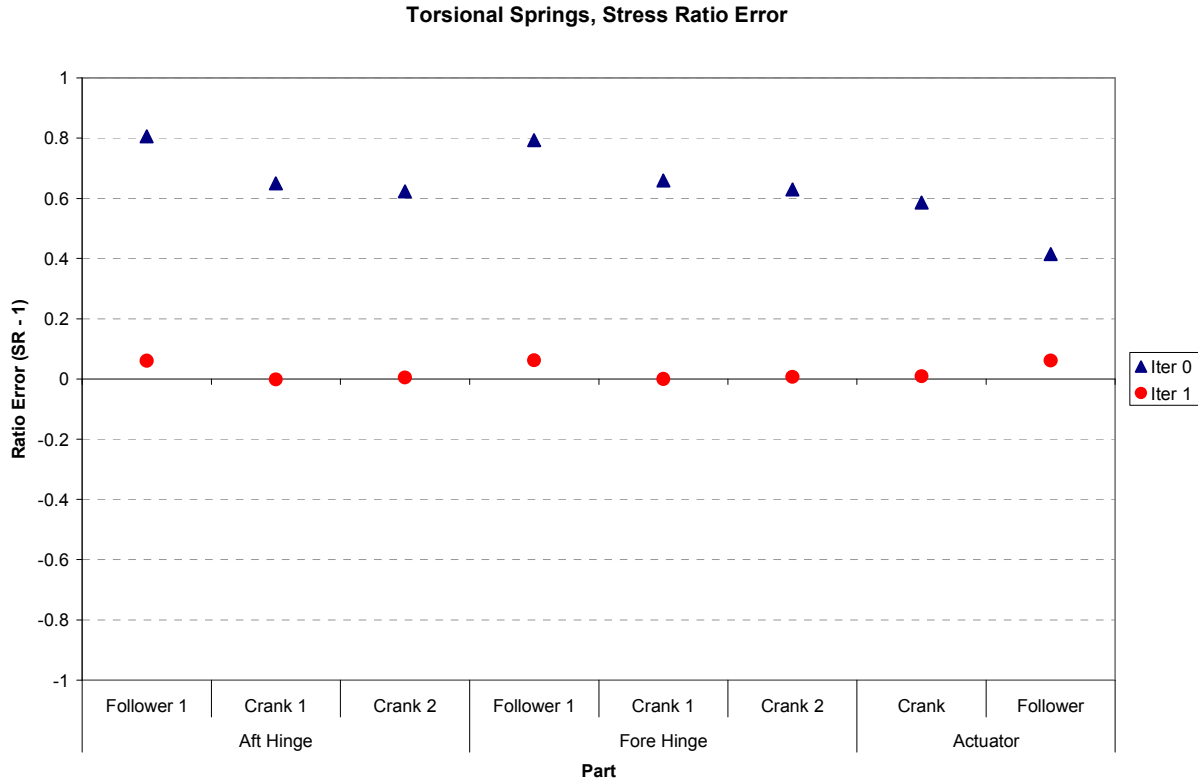


**Figure 10. Stress Ratio in Parts Represented by Torsional Springs**

Tolerance Analysis

To define the maximum length of the previously described misalignment vectors, actual tolerances must be gathered from each link’s engineering drawings. These values are shown in Table 4, along with the calculated maximum gap and maximum misalignment ( $\epsilon$ ). Comparing these values to the ANSI standard fit classes, most of the specified tolerances fall within a range most closely resembling the RC3 class for precision running fits [5].

**Table 4. Component Tolerance Values (mm)**

| Parent Part | Location | Child Part      | Nominal | +      | -      | Max Gap | Max $\epsilon$ |
|-------------|----------|-----------------|---------|--------|--------|---------|----------------|
| Door Rod    | End 1    | Rod End Bearing | 7.9248  | 0.0127 | 0.0000 | 0.0559  | 0.0279         |
|             |          | Shoulder Bolt   | 7.8918  | 0.0000 | 0.0102 |         |                |
|             | End 2    | Rod End Bearing | 7.9248  | 0.0127 | 0.0000 | 0.0559  | 0.0279         |
|             |          | Shoulder Bolt   | 7.8918  | 0.0000 | 0.0102 |         |                |
| Rod 1       | End 1    | Rod End Bearing | 7.9248  | 0.0127 | 0.0000 | 0.0559  | 0.0279         |
|             |          | Shoulder Bolt   | 7.8918  | 0.0000 | 0.0102 |         |                |
|             | End 2    | Rod End Bearing | 7.9248  | 0.0127 | 0.0000 | 0.0686  | 0.0343         |
|             |          | Pin             | 7.8816  | 0.0000 | 0.0127 |         |                |
| Follower 1  | Base     | Flanged Bushing | 12.7000 | 0.0127 | 0.0127 | 0.0686  | 0.0343         |
|             |          | Shoulder Bolt   | 12.6543 | 0.0000 | 0.0102 |         |                |
| Rod 2       | End 1    | Rod End Bearing | 7.9248  | 0.0127 | 0.0000 | 0.0559  | 0.0279         |
|             |          | Shoulder Bolt   | 7.8918  | 0.0000 | 0.0102 |         |                |
|             | End 2    | Rod End Bearing | 7.9248  | 0.0127 | 0.0000 | 0.0559  | 0.0279         |
|             |          | Shoulder Bolt   | 7.8918  | 0.0000 | 0.0102 |         |                |
| Follower 2  | Base     | Flanged Bushing | 12.7000 | 0.0127 | 0.0127 | 0.0686  | 0.0343         |
|             |          | Pin             | 12.6543 | 0.0000 | 0.0102 |         |                |
|             | Door     | Flanged Bushing | 12.7000 | 0.0127 | 0.0127 | 0.0686  | 0.0343         |
|             |          | Pin             | 12.6543 | 0.0000 | 0.0102 |         |                |
| Act. Rod    | End 1    | Rod End Bearing | 7.9248  | 0.0127 | 0.0000 | 0.0559  | 0.0279         |
|             |          | Shoulder Bolt   | 7.8918  | 0.0000 | 0.0102 |         |                |
|             | End 2    | Rod End Bearing | 7.9248  | 0.0127 | 0.0000 | 0.0559  | 0.0279         |
|             |          | Shoulder Bolt   | 7.8918  | 0.0000 | 0.0102 |         |                |
| Tube Shaft  | End 1    | Flanged Bushing | 41.2750 | 0.0127 | 0.0127 | 0.1067  | 0.0533         |
|             |          | Flanged Bushing | 41.2064 | 0.0000 | 0.0254 |         |                |
|             | Mid      | Flanged Bushing | 33.3375 | 0.0127 | 0.0127 | 0.1067  | 0.0533         |
|             |          | Flanged Bushing | 33.2689 | 0.0000 | 0.0254 |         |                |
|             | End 2    | Flanged Bushing | 22.2250 | 0.0127 | 0.0127 | 0.1067  | 0.0533         |
|             |          | Flanged Bushing | 22.1564 | 0.0000 | 0.0254 |         |                |

After applying the contents of Table 4 in the MATLAB optimization code, the maximum possible motion of the door's edge from its nominal location is 6.375 mm (0.251 in). If this motion is applied in both directions, then the maximum possible total mechanism backlash due to joint tolerances allows for 12.75 mm (0.502 in) of motion at the door's edge.

**Stress Analysis**

The stress results for each component after one iteration (used to find the “ $\sigma$  ratio[1]” values in Table 2 and Table 3), are shown below in Table 5 and Table 6. These values represent the predicted stress induced by a 25.4 mm (1 in) movement of the door's outboard edge, with the DDM actuator crank fixed. To calculate factor of safety (FS) values, an allowable stress of 703 MPa (102 ksi) was assumed.

**Table 5. Stress Results After 1 Iteration, Parts in Bending**

| Location   | Part       | Deflection (deg) | M (N·m)   | F (N)     | Displacement LBC   |      | Force LBC          |      | $\sigma$ ratio[j] | $\sigma$ ratio[j-1] |
|------------|------------|------------------|-----------|-----------|--------------------|------|--------------------|------|-------------------|---------------------|
|            |            |                  |           |           | FEA $\sigma$ (MPa) | FS   | FEA $\sigma$ (MPa) | FS   |                   |                     |
| Aft Hinge  | Follower 1 | 1.85E+00         | 2.34E+04  | 1.01E+05  | 1.44E+03           | 0.49 | 1.36E+03           | 0.52 | 1.061             | 1.806               |
|            | Crank 1    | 3.83E-01         | 2.27E+03  | 1.56E+04  | 5.12E+02           | 1.37 | 5.12E+02           | 1.37 | 0.999             | 1.650               |
|            | Crank 2    | -3.15E-01        | -2.38E+03 | -2.45E+04 | 5.38E+02           | 1.31 | 5.36E+02           | 1.31 | 1.005             | 1.624               |
| Fore Hinge | Follower 1 | 1.52E+00         | 1.92E+04  | 8.32E+04  | 1.19E+03           | 0.59 | 1.12E+03           | 0.63 | 1.062             | 1.793               |
|            | Crank 1    | 3.11E-01         | 1.84E+03  | 1.26E+04  | 4.16E+02           | 1.69 | 4.16E+02           | 1.69 | 1.000             | 1.660               |
|            | Crank 2    | -5.87E-01        | -4.43E+03 | -4.56E+04 | 1.00E+03           | 0.70 | 9.93E+02           | 0.71 | 1.007             | 1.630               |
| Actuator   | Crank      | -2.48E-01        | -1.80E+03 | -2.47E+04 | 6.52E+02           | 1.08 | 6.46E+02           | 1.09 | 1.010             | 1.585               |
|            | Follower   | 3.91E-01         | 2.71E+03  | 3.35E+04  | 9.51E+02           | 0.74 | 8.96E+02           | 0.78 | 1.062             | 1.415               |

**Table 6. Stress Results After 1 Iteration, Parts in Tension/Compression**

| Location   | Part       | Deflection (mm) | F (N)     | Displacement LBC   |      | Force LBC          |      | $\sigma$ ratio[i] | $\sigma$ ratio[i-1] |
|------------|------------|-----------------|-----------|--------------------|------|--------------------|------|-------------------|---------------------|
|            |            |                 |           | FEA $\sigma$ (psi) | FS   | FEA $\sigma$ (psi) | FS   |                   |                     |
| Aft Hinge  | Follower 1 | 1.10E-01        | 8.42E+04  | 2.58E+02           | 2.73 | 2.55E+02           | 2.76 | 1.011             | 1.016               |
|            | Rod 1      | -9.77E-02       | -2.51E+04 | 3.48E+02           | 2.02 | 3.47E+02           | 2.03 | 1.004             | 0.636               |
|            | Rod 2      | 1.37E-01        | 3.41E+04  | 2.58E+02           | 2.73 | 2.59E+02           | 2.72 | 0.997             | 0.835               |
|            | Door Rod   | -4.26E-01       | -1.06E+05 | 8.07E+02           | 0.87 | 8.00E+02           | 0.88 | 1.009             | 0.832               |
| Fore Hinge | Follower 1 | 9.00E-02        | 6.92E+04  | 2.12E+02           | 3.31 | 2.10E+02           | 3.36 | 1.013             | 1.065               |
|            | Rod 1      | -7.99E-02       | -2.06E+04 | 2.84E+02           | 2.48 | 2.83E+02           | 2.48 | 1.002             | 0.632               |
|            | Rod 2      | 2.55E-01        | 6.36E+04  | 4.78E+02           | 1.47 | 4.81E+02           | 1.46 | 0.994             | 0.833               |
|            | Door Rod   | -3.50E-01       | -8.72E+04 | 6.61E+02           | 1.06 | 6.60E+02           | 1.07 | 1.001             | 0.831               |
| Actuator   | Rod        | -3.44E-01       | -7.56E+04 | 1.73E+03           | 0.41 | 1.74E+03           | 0.40 | 0.996             | 1.271               |

Although these results do show some components with factors of safety less than one, this does not necessarily mean that closure of the ETD during STS-118 would have resulted in yield. Because the actual rigged door sag was not known at the time, this analysis did not produce a definitive prediction of additional stress induced in the door drive linkage. Because the minimum computed factor of safety for 25.4 mm (1 in) of door motion was 0.41, the door could be forced to move up to 10.16 mm (0.40 in) at its outboard edge before allowable stresses would be reached.

### Resolution of Door Closure, Future Work

After reviewing both the results outlined here and photographs taken during the orbiter's rendezvous pitch maneuver, it was determined that the only action necessary to ensure proper door closure was a cycling of the uplatches. During this procedure, the door drive was once more operated in the closed direction, and all closed indications were received through telemetry. To complement the analyses described in this paper, actual rigging data from the orbiter *Endeavour* taken before STS-118 could be used to reach a better estimate of stress in the DDM. Predicted stresses could then potentially be further confirmed through experimentation using a training mockup version of the DDM.

### Conclusions

Through the use of MSC/ADAMS, a flexible multi-body dynamic simulation of the ETD DDM was able to be quickly constructed and used to find linkage deflections. The advantage of this type of analysis is its relative simplicity compared to a full FEA model of the DDM, combined with preserved accuracy of mechanism kinematics. This simplicity allows for rapid construction of the model in addition to a reduction in computer computation time required. Although complex geometry is reduced to lumped equivalent stiffnesses, the analyst has the ability to select each flexible degree of freedom that will be of primary interest and include it in the model. The stiffness used for each of these individual degrees of freedom may then be verified using FEA and updated as necessary.

### Acknowledgement

We would like to dedicate this paper to the memory of Marlon C. Batey. Marlon worked as an aerospace engineer in the Mechanical Systems Branch of NASA Langley Research Center over the past three years. Without his contributions to the team, none of the work described here would have been possible. In addition to his diligence and motivation, it was always a pleasure to work with him. Marlon has been and will be greatly missed.

### References

1. Don Picetti, Thermal Analysis and Test Results for ET Door Paint Striping, Boeing Orbiter Element, S063244, Daily PRCB Presentation
2. Rao, Singiresu S. Mechanical Vibrations, Fourth Edition, Pearson Prentice Hall, 2004

- 3 . Brinkworth, D. "ET/Orbiter Umbilical Door Mechanism Installation and Rigging Procedure", Space Division Rockwell International, Doc. No. ML0308-0058 rev. C, 1982
- 4 . Chase, Kenneth W.; Gao, Jinsong; Magleby, Spencer P. "General 2-D Tolerance Analysis of Mechanical Assemblies with Small Kinematic Adjustments", Journal of Design and Manufacturing, v 5 n 4, 1995
- 5 . Oberg, Erik. Machinery's Handbook, 24<sup>th</sup> Edition. Industrial Press, 1992